Published in "Nature Physics 3: 86 - 789, 2007"
which should be cited to refer to this work.

Impurity-stabilized solid ^{4}He below the solidification pressure of pure helium

P. MOROSHKIN, A. HOFER, S. ULZEGA* AND A. WEIS†

Département de Physique, Université de Fribourg, Chemin du Musée 3, 1700 Fribourg, Switzerland

***Present address: EPFL, 1015 Lausanne, Switzerland**

†**e-mail: antoine.weis@unifr.ch**

The modification of melting temperatures and pressures by dissolved impurities is well known in classical fluids. However, to our knowledge such effects have never been studied in quantum solids because of the difficulties in introducing impurities into such crystals that exist only at cryogenic temperatures, and, in the case of ^{4}He, at pressures exceeding 25 bar. Here, we present an effect that occurs during the melting of solid ^{4}He doped with nanoscopic impurities (alkali atoms, clusters, ions and electrons): the doped part of the crystal remains solid under conditions at which pure helium is liquid. Using interferometry, we found that the density of the solid structure lies between the densities of pure liquid and pure solid helium. We tentatively interpret the solid structure as being an aggregation of positively charged particles and electron bubbles.

The coexistence of a ^{4}He crystal with superfluid ^{4}He is a model system for investigating fundamental aspects of the growth and melting of quantum crystals. Many subtle effects at the crystal–liquid interface have been studied in the past, such as faceting and propagation of crystallization waves (reviewed in ref. 1), interface motion under the action of acoustic waves[2] or confined electrons[3] and instability induced by a non-hydrostatic stress[4]. The role of ^{3}He impurities was discussed in connection with the formation of supersolid ^{4}He (refs 5,6).

In the past decade, we have developed a laser ablation technique for doping a ^{4}He crystal with atomic impurities. Our (recently reviewed[7]) main research activity is devoted to optical and magnetic resonance spectroscopy of atomic, molecular and exciplex defects, both in body-centred-cubic (b.c.c.) and in hexagonal close-packed (h.c.p.) ^{4}He crystals. The doped part of the crystal has approximately the shape of a vertical cylindrical column of bluish colour, which can be observed through a side window of the cell (Fig. 1a–d).

When the crystal pressure is slowly decreased, an interesting phenomenon is observed during the solid–liquid phase transition. Fig. 1a,b shows the doped crystal in the h.c.p. and b.c.c. phases respectively. Whereas the h.c.p. phase is perfectly homogeneous and transparent, the b.c.c. phase has a polycrystalline structure and light refraction at the grain boundaries gives the sample a turbid, albeit not completely opaque, appearance (Fig. 1b). The crystal melts from top to bottom when the pressure is further released. The well-visible liquid–solid phase boundary moves downwards when the pressure is lowered. In Fig. 1c, the liquid level has dropped below the upper end of the doped column. Most remarkably, the doped column remains a solid and stable structure protruding into the liquid until all surrounding helium is liquefied (Fig. 1d), while still under pressure. Under those conditions the structure remains unchanged for at least half an hour. A further relief of pressure makes the structure break up into many smaller parts which then float to the bottom of the pressure cell (Fig. 2). We will refer to the solid structure in the liquid matrix as an 'iceberg'.

We have observed similar structures in crystals doped by ablation from targets of caesium, rubidium or their 50/50 mixture, which all behave similarly. To better understand the nature of the icebergs, we have carried out the investigation reported below.

The colour of the sample (Fig. 1) is due to a broad absorption band centred around 750 nm for Cs and 640 nm for Rb (Fig. 3) that is typical for plasmon resonances in metallic nanoparticles[8]. The spectral dependence of the extinction coefficient depends on the cluster size and on the complex dielectric function, $\epsilon(\lambda)$, of the metal. It is described by Mie theory[9] for small particle sizes ($R_{\mathrm{cl}} \ll \lambda$). Using dielectric functions from ref. 10, we have modelled the extinction spectra by assuming spherically shaped clusters and fitted the experimental spectra by adjusting the radii, R_{cl}, and density distribution, $N_{\mathrm{cl}}(R_{\mathrm{cl}})$, of the Rb_n and Cs_n clusters (Fig. 3). For caesium, a best fit with the experimental spectrum is obtained for an average cluster radius of $\langle R_{\mathrm{cl}} \rangle = 41\,\mathrm{nm}$, a width of the distribution (full-width at half-maximum) of $\Delta R_{\mathrm{cl}} = 50\,\mathrm{nm}$ and a total cluster density $N_{\mathrm{cl}} = 3.3 \times 10^9\,\mathrm{cm}^{-3}$ (assuming a 3 mm diameter of the doped part of the crystal). The corresponding parameters for rubidium are $\langle R_{\mathrm{cl}} \rangle = 10\,\mathrm{nm}$, $\Delta R_{\mathrm{cl}} = 41\,\mathrm{nm}$ and $N_{\mathrm{cl}} = 2.5 \times 10^{10}\,\mathrm{cm}^{-3}$.

We have determined the density of the doped sample from the index of refraction measured with a Mach–Zehnder interferometer. The index of refraction of pure solid helium is $n_{\mathrm{He}} = \sqrt{1 + 4\pi\alpha_{\mathrm{He}}(\lambda)\rho} = 1.03716$ for a molar polarizability $\alpha_{\mathrm{He}}(\lambda) = 0.125\,\mathrm{cm}^3\,\mathrm{mol}^{-1}$ (ref. 11) (at $\lambda = 546\,\mathrm{nm}$) and a molar density $\rho = 4.82 \times 10^{-2}\,\mathrm{mol\,cm}^{-3}$ (at $p = 30\,\mathrm{bar}$ and $T = 1.5\,\mathrm{K}$). The index of refraction, n_{cl}, of nanoparticles suspended in a dielectric matrix with index of refraction n_{He} can be calculated from Mie theory. It can be shown—using N_{cl} and R_{cl} inferred from the extinction measurement—that the clusters change the index of refraction by $\Delta n_{\mathrm{cl}} = 2 \times 10^{-6}$, which induces a further phase shift of only $0.01 \times 2\pi$ and hence does not affect the fringe pattern compared to the pattern observed with pure helium.

The first and second rows of Fig. 1 were obtained with different samples (Rb in the first row, Cs in the second row), but corresponding pictures in each column were recorded during similar phases of the melting process. Interferograms taken in doped solid He are indistinguishable from those taken in pure liquid or pure solid helium and reveal no structure that could

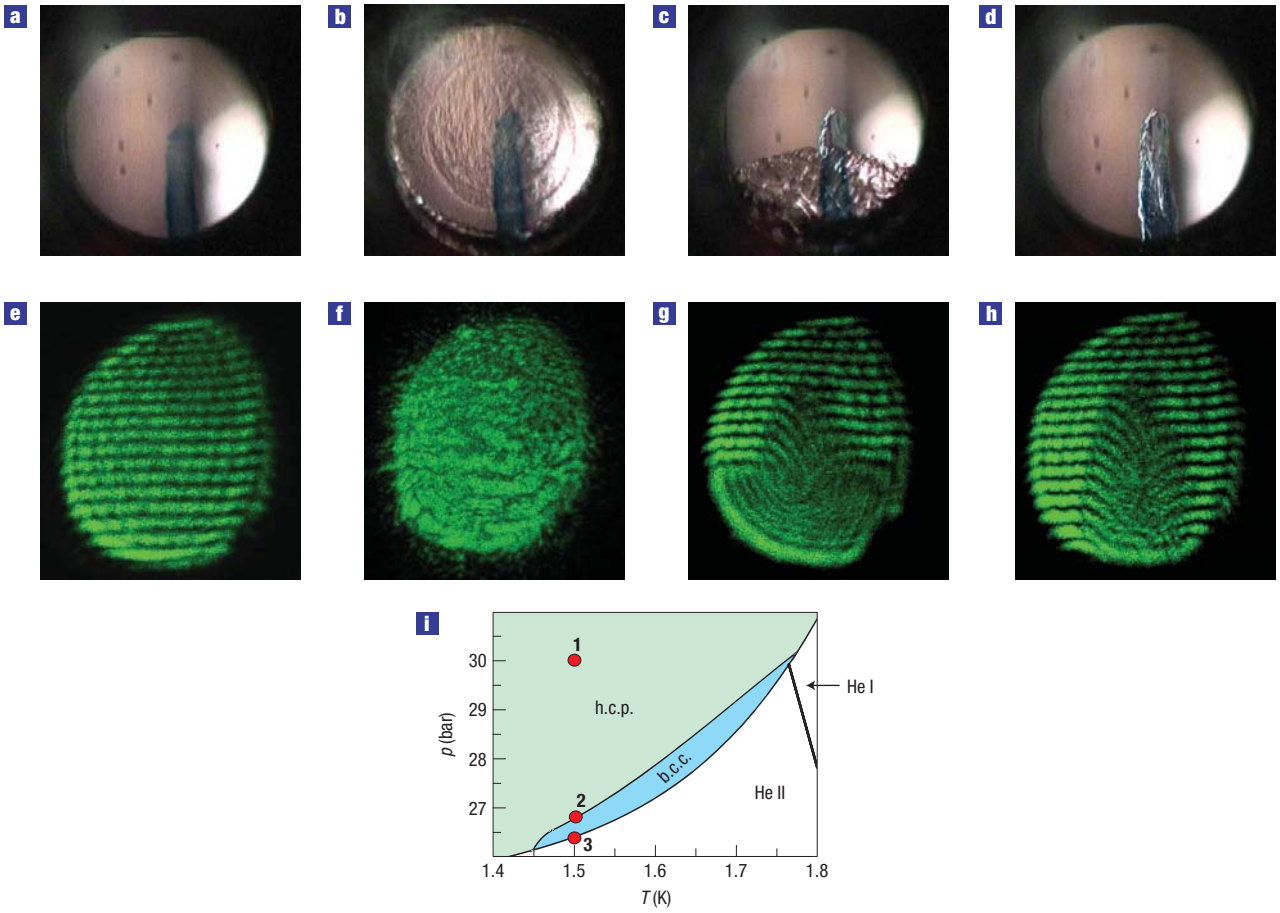

Figure 1 Appearance of iceberg structure during melting of a doped ^{4}He crystal. a–h, Photographs of Rb-doped (**a–d**) and interferograms of Cs-doped (**e–h**) He taken through a 2-cm-diameter window during controlled pressure release at $T = 1.5$ K. **i**, Phase diagram showing the corresponding experimental conditions as points. **a**,**e** at point 1: h.c.p. crystalline phase at 30 bar; **b**,**f** at point 2: transition from h.c.p. to b.c.c. at 26.8 bar; **c**,**g** at point 3: b.c.c.–liquid phase transition at 26.4 bar; **d**,**h** at point 3: liquid He at 26.4 bar, just at the end of the phase transition. The column-like structure in the centre (iceberg) corresponds to the part doped with Cs/Rb.

be associated with the dopants (atomic or cluster). A typical fringe pattern obtained with Cs doped (h.c.p.) solid He is shown in Fig. 1e.

Lowering the He pressure in the cell results in a uniform upward motion of the fringe pattern. During the phase transition (h.c.p. to b.c.c. and also b.c.c. to liquid) the sample becomes inhomogeneous, owing to the coexistence of the two involved phases (Fig. 1b and lower part of Fig. 1c) and the fringes disappear (Fig. 1f and lower part of Fig. 1g).

When the pressure is further released, the crystal starts to melt and the two phases separate: the solid occupies the lower part of the cell, and the liquid the upper part, as shown in Fig. 1c,g. The iceberg structure rises from the b.c.c. phase into the He liquid (which is homogeneously transparent) yielding a horizontal fringe pattern, whereas the fringes are deformed in the region of the iceberg. Finally, Fig. 1d,h shows the iceberg after the surrounding helium is completely liquefied.

The fringes in the region of the iceberg are strongly deformed, indicating that the refractive index of the iceberg differs from that of the surrounding liquid helium. The curvature of the fringes is related to the variation of the thickness of the (approximately cylindrical) iceberg across the picture, and the fringe shift (with respect to its position in the liquid) reaches a maximum in the centre of the iceberg, where it is thickest. As discussed above, the dopants (atoms and/or clusters) have a negligible contribution to the refractive index, which is thus determined only by the He density. From the downward bending of the fringes and their upward motion during pressure release, we conclude that the iceberg density is larger than that of liquid helium.

The fringes produced by a ≈3-mm-thick slab of helium (the iceberg diameter) move by approximately 16 fringe periods when going from solid to liquid, as is easily estimated on the basis of the refractive indices of helium given above. From Fig. 1g,h, we can estimate a maximal deformation of the pattern to be 3 to 4 fringe periods in the centre of the iceberg. This leads us to conclude that the density of the iceberg lies somewhere between the densities of liquid and solid helium, although closer to the liquid density.

The solid structure in caesium-doped helium reported here has several common features with the macroscopic solid structures, called impurity-helium solids, investigated in refs 12–15. In those experiments, a helium gas jet doped with molecular or atomic impurities was directed into liquid helium. On condensation in the helium bath, the gas mixture forms a macroscopic highly porous structure composed of frozen impurity clusters surrounded by a relatively thin shell of solid helium[14,15]. According to a theoretical model presented in ref. 12, the solidification of He in those structures, that is, the attachment of He atoms to the impurity centre, is due to the van der Waals attraction between the

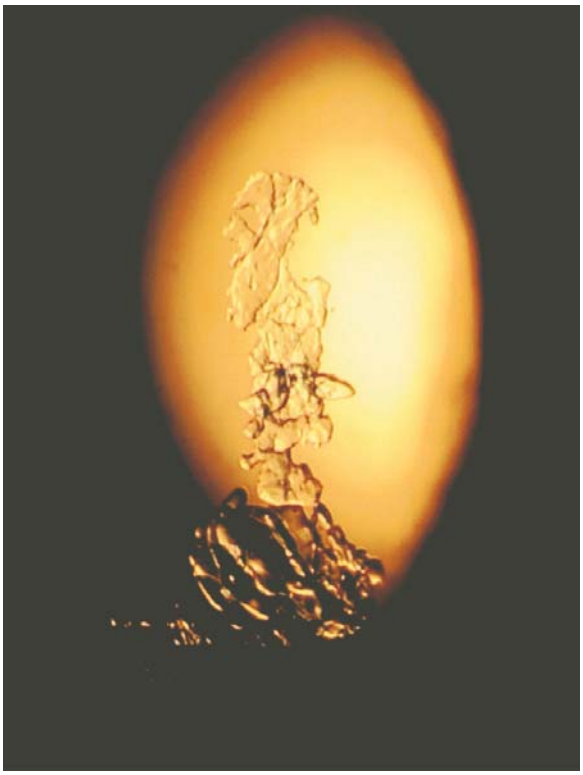

Figure 2 Caesium-doped iceberg in liquid helium during its disintegration. The shape of the illuminated region results from the oblique view through two aligned windows. $T = 1.5$ K, $p = 26.4$ bar.

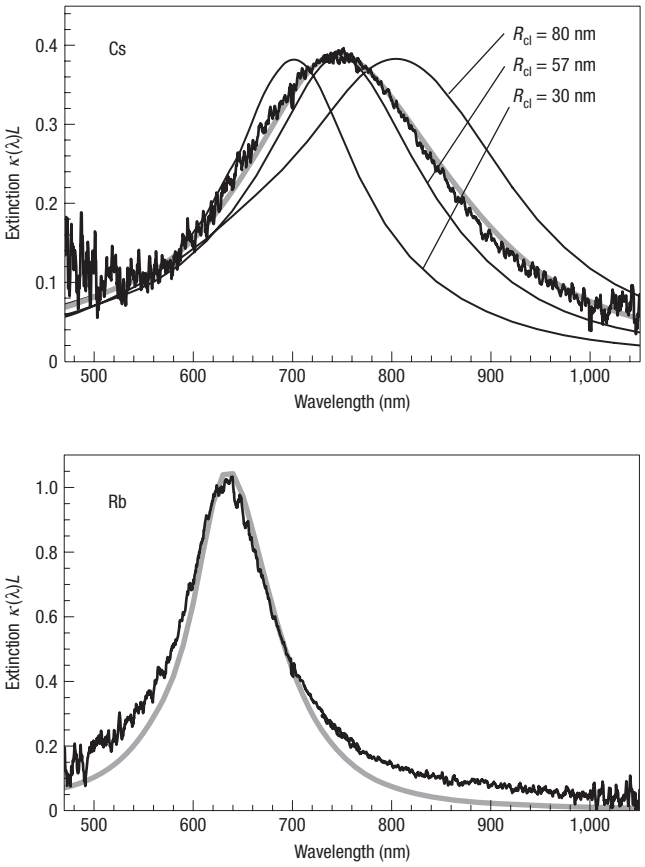

Figure 3 Extinction spectra of Cs- and Rb-doped solid He. The noisy curves are experimental data and the thick line is the result from Mie theory with a gaussian distribution of cluster sizes as discussed in the text. For Cs we also show the Mie results for monodisperse clusters (thin lines).

impurity atoms or molecules (which have paired electrons) and the surrounding helium atoms.

The structure observed here has a different underlying binding mechanism. The strong repulsion (due to the Pauli principle) between the unpaired Cs/Rb valence electron and the closed *S*-shell of a He atom dominates over the attractive van der Waals force[16]. Moreover, the estimated[17] number density of Cs atoms (10^8–10^9 cm^{-3}) is many orders of magnitude smaller than the dopant concentrations used in the experiments with impurity-helium solids (about 10^{20} cm^{-3}). Alkali clusters also have a very low number density, and the electron density on their surface is so high that He atoms cannot approach close enough to experience a van der Waals attraction[18], as demonstrated by the non-wetting of solid Cs by superfluid ^{4}He (ref. 19). It is therefore very unlikely that neutral particles can hold together such a large amount of He atoms and the observed iceberg structure must be due to another type of impurities produced during ablation. These impurities are not detected by our spectroscopic (extinction, laser induced fluorescence[7]) and interferometric measurements.

On the basis of these facts, we assume that charged particles are responsible for the iceberg formation. It is well known[20,21] that alkali ions in liquid He attract He atoms via electrostriction and form so-called snowballs—complexes consisting of one alkali ion surrounded by a spherical shell of He atoms whose local density is so high that it is solid. According to recent theoretical studies[22,23], up to 17 He atoms can be bound to a single Cs^+ ion in liquid He. It is also well known that the electrostriction produced by an externally applied inhomogeneous electric field in liquid helium at appropriate temperature and pressure can initiate He crystal nucleation[24]. Both atomic and cluster ions can be produced by the laser ablation from a metallic surface and are thus probably present in our samples. The extinction spectra in Fig. 3 contain contributions from neutral and positively charged clusters as the plasmon resonance frequencies of large clusters depend on the number of electrons, N_e, and are thus insensitive to their degree of ionization. Highly charged clusters break up into smaller weakly charged clusters by Coulomb explosion. The density of charged clusters is thus smaller than N_{cl} determined from Fig. 3. It is likely—although, to our knowledge not studied—that charged clusters also form snowballs like atomic ions do. We therefore believe that atomic (and eventually cluster) ions play a dominant role in binding He atoms together. Unfortunately, the absorption lines of Cs^+ and Rb^+ ions lie in the deep ultraviolet part of the spectrum, not accessible to our spectrometer.

Our observation of electric-field-induced currents in doped crystals[25] points to the presence of charges. Another manifestation of the presence of charged impurities is observed when the sample (iceberg) is destroyed by releasing He pressure in the presence of an electric field. After the melting of surrounding solid He, fragments of different sizes start to split off the iceberg and to move towards one of the high-voltage electrodes, where they stick and stay attached until the complete destruction. At some point, the whole iceberg splits into two groups of fragments attracted each by one of the electrodes.

Crystalline structures formed by ionic snowballs were recently observed[26] in experiments with He^+ ions in liquid He which form

two-dimensional crystals when confined by electric fields. The iceberg structure reported here is stable without any external field. We suggest that the repulsive Coulomb interaction between the ions is compensated by the attractive forces due to electrons—other negatively charged particles are unlikely to be present—distributed in the same doped volume. Indeed, the laser ablation produces equal amounts of positive and negative charges and the resulting iceberg as a whole is electrically neutral. The recombination of the charged particles, although very efficient in the gas phase, is strongly suppressed in condensed He owing to the stabilizing effect of the snowball shell surrounding each positive ion and the bubble structure of the electron[27]. From the Pauli principle, the electron experiences a strong repulsion by the closed *S*-shells of the He atoms and cannot come close enough to the snowball core, thereby suppressing recombination.

In summary, we believe that the iceberg consists of the aggregation of positively charged particles and electron bubbles probably assisted by surface tension[28]. Whether these particles form a disordered or an ordered (poly-)crystalline structure is not clear. Future studies using infrared spectroscopy of electron bubbles or a measurement of plasma oscillations, for example, may provide more detail on the nature of the iceberg.

METHODS

Experiments were carried out at 1.5 K over a range of pressures covering 26 to 36 bar. The phase diagram of ^{4}He (Fig. 1i) shows that at 1.5 K and 26.4 bar, superfluid He solidifies in a b.c.c. crystalline structure, which then makes a phase transition to a h.c.p. structure at 26.8 bar.

The implantation technique is described in detail in refs 7,17. A helium crystal is grown inside a pressure cell (inner volume $\approx$ 200 ml) by condensing and then solidifying pressurized helium gas from an external reservoir. The cell is immersed in a helium bath kept at 1.5 K by pumping on the bath. Four lateral windows and a top window provide optical access from three orthogonal directions. The solid host matrix is doped with Cs/Rb atoms by means of laser ablation with the second harmonic of a pulsed frequency-doubled Nd:YAG laser focused through the top window onto a solid alkali metal target at the bottom of the cell.

For the extinction measurements, a collimated beam of white light from a halogen lamp was sent through the sample and the spectrum, $I(\lambda)$, of the transmitted light was analysed by a grating spectrograph equipped with a CCD (charge-coupled device) camera. The extinction coefficient is defined by $\kappa(\lambda)L = -\ln I(\lambda)/I_0(\lambda)$, where L is the sample thickness and $I_0(\lambda)$ is a reference spectrum recorded after the complete melting of the crystal.

The index of refraction of the sample is measured using a two-beam Mach–Zehnder interferometer illuminated with a beam from a green laser pointer (532 nm) expanded to the size of the cell windows (2 cm diameter). One of the interferometer arms crosses the sample. A small angle is introduced between the two interfering beams to obtain a pattern of 10–20 horizontally oriented interference fringes covering both the doped and the undoped parts of the matrix. The fringe pattern is projected onto a screen and photographed with a digital camera (Fig. 1e–h).

References

1. Balibar, S., Alles, H. & Parshin, A. Ya. The surface of helium crystals. *Rev. Mod. Phys.* **77**, 317–370 (2005).
2. Nomura, R., Kimura, S., Ogasawara, F., Abe, H. & Okuda, Y. Orientation dependence of interface motion in ^{4}He crystals induced by acoustic waves. *Phys. Rev. B* **70**, 054516 (2004).
3. Savignac, D. & Leiderer, P. Charge-induced instability of the ^{4}He solid-superfluid interface. *Phys. Rev. Lett.* **49**, 1869–1872 (1982).
4. Torii, R. H. & Balibar, S. Helium crystals under stress: The Grinfeld instability. *J. Low Temp. Phys.* **89**, 391–400 (1992).
5. Kim, E. & Chan, M. H. W. Probable observation of a supersolid helium phase. *Nature* **427**, 225–227 (2004).
6. Prokof'ev, N. What makes a crystal supersolid? *Adv. Phys.* **56**, 381–402 (2007).
7. Moroshkin, P., Hofer, A., Ulzega, S. & Weis, A. Spectroscopy of atomic and molecular defects in solid ^{4}He using optical, microwave, radio frequency, magnetic and electric fields. *Low Temp. Phys.* **32**, 981–998 (2006).
8. Mochizuki, S., Inozume, K. & Ruppin, R. Spectroscopic studies of rubidium vapour zone produced by thermal evaporation in noble gas. *J. Phys. Condens. Matter* **11**, 6605–6619 (1999).
9. van de Hulst, H. C. *Light Scattering by Small Particles* (Dover, New York, 1981).
10. Smith, N. V. Optical constants of rubidium and cesium from 0.5 to 4.0 eV. *Phys. Rev. B* **2**, 2840–2848 (1970).
11. Edwards, M. H. Refractive index of ^{4}He: Saturated vapor. *Phys. Rev.* **108**, 1243–1245 (1957).
12. Gordon, E. B. *et al.* Metastable impurity-helium solid phase. Experimental and theoretical evidence. *Chem. Phys.* **170**, 411–426 (1993).
13. Boltnev, R. E. *et al.* Luminescence of nitrogen and neon atoms isolated in solid helium. *Chem. Phys.* **189**, 367–382 (1994).
14. Kiselev, S. I. *et al.* Structural studies of impurity-helium solids. *Phys. Rev. B* **65**, 024517 (2001).
15. Gordon, E. B. Impurity condensation in liquid and solid helium. *Low Temp. Phys.* **30**, 756–762 (2004).
16. Pascale, J. Use of l-dependent pseudopotential in the study of alkali-metal-atom-He systems. The adiabatic molecular potential. *Phys. Rev. A* **28**, 632–644 (1983).
17. Arndt, M., Dziewior, R., Kanorsky, S., Weis, A. & Hänsch, T. W. Implantation and spectroscopy of metal atoms in solid helium. *Z. Phys. B* **98**, 377–381 (1995).
18. Cheng, E., Cole, M. W., Dupont-Roc, J., Saam, W. F. & Treiner, J. Novel wetting behavior in quantum films. *Rev. Mod. Phys.* **65**, 557–567 (1993).
19. Nacher, P. J. & Dupont-Roc, J. Experimental evidence for nonwetting with superfluid helium. *Phys. Rev. Lett.* **67**, 2966–2969 (1991).
20. Cole, M. W. & Bachman, R. A. Structure of positive impurity ions in liquid helium. *Phys. Rev. B* **15**, 1388–1394 (1977).
21. Glaberson, W. I. & Johnson, W. W. Impurity ions in liquid helium. *J. Low Temp. Phys.* **20**, 313–338 (1975).
22. Buzzacchi, M., Galli, D. E. & Reatto, L. Alkali ions in superfluid ^{4}He and structure of the snowball. *Phys. Rev. B* **64**, 094512 (2001).
23. Rossi, M., Verona, M., Galli, D. E. & Reatto, L. Alkali and alkali-earth ions in ^{4}He systems. *Phys. Rev. B* **69**, 212510 (2004).
24. Keshishev, K. O., Parshin, A. Y. & Babkin, A. V. Experimental detection of crystallization waves in He-4. *JETP Lett.* **30**, 56–59 (1979).
25. Ulzega, S., Hofer, A., Moroshkin, P. & Weis, A. Measurement of the forbidden electric tensor polarizability of Cs atoms trapped in solid ^{4}He. *Phys. Rev. A* **75**, 042505 (2007).
26. Elliott, P. L., Pakes, C. I., Skrbek, L. & Vinen, W. F. Capillary-wave crystallography: Crystallization of two-dimensional sheets of He^+ ions. *Phys. Rev. B* **61**, 1396–1409 (2000).
27. Jortner, J., Kestner, N. R., Rice, S. A. & Cohen, M. H. Study of the properties of an excess electron in liquid helium. *J. Chem. Phys.* **43**, 2614–2625 (1965).
28. Cole, M. W. & Sluckin, T. J. Nucleation of freezing by charged particles. I. Thermodynamics. *J. Chem. Phys.* **67**, 746–750 (1977).

Acknowledgements

This work was supported by grant No. 200020–103864 of the Schweizerischer Nationalfonds. Correspondence and requests for materials should be addressed to A.W.